DOI: 10.1002/cmdc.200700209

Organometallic Ruthenium Inhibitors of Glutathione-*S*-Transferase P1-1 as Anticancer Drugs

Wee Han Ang,*[a] Anastasia De Luca,[b] Catherine Chapuis-Bernasconi,[c] Lucienne Juillerat-Jeanneret,[c] Mario Lo Bello,*[b] and Paul J. Dyson*[a]

Ruthenium–arene complexes conjugated to ethacrynic acid were prepared as part of a strategy to develop novel glutathione-S-transferase (GST) inhibitors with alternate modes of activity through the organometallic fragment, ultimately to provide targeted ruthenium-based anticancer drugs. Enzyme kinetics and electrospray mass spectrometry experiments using GST P1-1 and its cysteine-modified mutant forms revealed that the complexes are effective enzyme inhibitors, but they also rapidly inactivate the enzyme by covalent binding at Cys 47 and, to a lesser extent, Cys 101. They are highly effective against the GST Pi-positive A2780 and A2780cisR ovarian carcinoma cell lines, are among the most effective ruthenium complexes reported so far, and target ubiquitous GST Pi overexpressed in many cancers.

Introduction

Glutathione-*S*-transferase (GST, EC 2.5.1.18) comprises an important class of biotransformation enzymes, the main function of which is the detoxification of toxic compounds. The key role of cytosolic GST is to catalyze the nucleophilic attack of reduced glutathione (GSH) on the electrophilic center of toxic compounds of both endogenous and xenobiotic origin, the first step in the mercapturic acid pathway that leads to elimination of the toxic compounds.[1] GST constitutes an important part of the cellular defense against external insult, and several studies have also found a strong link between drug resistance and the overexpression of GST enzymes, particularly GST Pi and GST Alpha classes.[2] In addition, the GST P1-1 isozyme, a member of the GST Pi enzyme class, is known to regulate the mitogen-activated protein (MAP) pathway, involved in cellular survival and death signaling.[3] A broad range of GST inhibitors, with varying degrees of isozyme-specificity, are known, and some of them have been systemically tested in combination with a range of alkylating agents against multiple drug-resistant (MDR) cancers as adjuvant therapeutics. In particular, ethacrynic acid (EA), a diuretic in clinical use, has been extensively studied and found to effectively inhibit all GST isozymes to varying extents (see Figure 1).[4]

The active site in the various classes of GST enzymes is constituted by the G site, the site of GSH binding, and the H site, for the binding of electrophilic substrates such as 1-chloro-2,4-dinitrobenzene (CDNB).[5] Of the various classes of GST enzymes, GST P1-1 is one of the more cysteine-rich GST isozymes, with four cysteine residues located at positions 14, 47, 101, and 169. It was previously shown that Cys 47 is located near the G site and is important for catalytic activity, as it is critical for the conformation and stability of the G site.[6] Cys 101 is located at the dimer interface and can form a disulfide bridge with Cys 47, leading to inactivation of the enzyme. Both Cys 47 and Cys 101 are known to be accessible to solvent molecules, whereas Cys 14 and Cys 169 are embedded within the hydrophobic regions and are less accessible.[7] We were therefore interested to study whether the inhibitory activity of organometallic ruthenium fragments could be modulated by conjugation

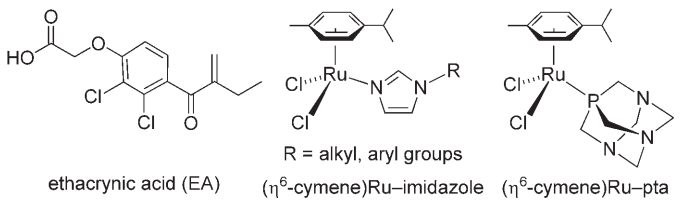

ethacrynic acid (EA) (η^6-cymene)Ru–imidazole complex (η^6-cymene)Ru–pta complex (RAPTA-C)

Figure 1. Ethacrynic acid and organometallic ruthenium–arene complexes investigated for anticancer properties.

[a] *Dr. W. H. Ang, Prof. P. J. Dyson*
Institut des Sciences et Ingénierie Chimiques
Ecole Polytechnique Fédérale de Lausanne (EPFL)
1015 Lausanne (Switzerland)
Fax: (+41) 21-693-9885
E-mail: weehan.ang@epfl.ch

[b] *A. De Luca, Prof. M. Lo Bello*
Department of Biology, University of Rome Tor Vergata
Via della Ricerca Scientifica snc, Rome 00133 (Italy)
Fax: (+39) 06-202-5450
E-mail: lobello@uniroma2.it

[c] *C. Chapuis-Bernasconi, Dr. L. Juillerat-Jeanneret*
University Institute of Pathology
Centre Hospitalier Universitaire Vaudois (CHUV)
1011 Lausanne (Switzerland)

to EA, as transition metals such as ruthenium have high binding affinity to sulfur groups. Furthermore, organometallic ruthenium complexes such as (η^6-arene)ruthenium imidazole complexes and (η^6-arene)ruthenium complexes with 1,3,5-triaza-7-phosphatricyclo[3.3.1.1]decane (pta) ligands (see Figure 1) are under active investigation as anticancer drugs and have been found to preferentially target tumor cells.[8–10] Thus, organometallic ruthenium complexes with GST-inhibitory functionality can potentially have enhanced antiproliferative activity.[10,11]

Accordingly, a series of ruthenium–EA complexes with analogous organometallic fragments were prepared and their interactions with GST P1-1 were investigated. Elucidation of the nature of their inhibitory activity was carried out with wild-type GST P1-1 and its cysteine-modified mutants. The ability of these complexes to inhibit cancer cell growth was also evaluated by using GST Pi-positive A2780 (cisplatin-sensitive) and A2780cisR (cisplatin-resistant) human ovarian carcinoma cell lines.

Results and Discussion

The main component of EA responsible for its GST-inhibitory activity is the phenolic group comprising the α,β-unsaturated conjugated carbonyl system and the 2,3-dichlorinated aromatic ring.[12] In contrast, the α-acetic acid group can be modified with minimal changes to the inhibitory activity of EA. Coupling of the EA moiety to organometallic ruthenium–arene fragments can be carried out with a range of linkers such as phosphino, amino, sulfido, and imidazole. We decided to use the imidazole linker because the chemistry of organometallic ruthenium–arene–imidazole complexes is well established, and their ability to inhibit cancer cell growth has also been extensively investigated (see Figure 1).[8,13]

EA–imidazole (EA–Im) **1** was prepared by amide condensation using the acid chloride derivative of EA and *N*-(3-aminopropyl)imidazole, followed by purification with flash column chromatography. EA–Im **1** was obtained as a hygroscopic oil that decomposes over time, presumably via dimerization at the α,β-unsaturated carbonyl bond. Therefore, freshly prepared EA–Im **1** was treated with (η^6-*p*-cymene)ruthenium precursors to yield the target organometallic ruthenium–EA complexes **2**–**4** (see Scheme 1), which are stable solids under ambient conditions. In addition, the structurally similar (η^6-*p*-cymene)ruthenium complex with *n*-butylimidazole RU-A (see Figure 1 center, R = *n*-butyl) was prepared and used as a reference in the biological experiments.

The complexes were characterized with ^{1}H and ^{13}C NMR, electrospray ionization mass spectrometry (ESIMS) and elemental analyses. ^{1}H and ^{13}C NMR resonances were assigned on the basis of heteronuclear single quantum correlation and heteronuclear multiple bond correlation experiments, and key assignments are listed in Table 1. Upon coordination of the organometallic Ru fragment, the characteristic resonances due to the capped cymene ligand, namely H1′ (singlet), H6′ (septet), and H7′ (doublet), were clearly observed whereas the resonances of the protons on the EA moiety remained largely unchanged.

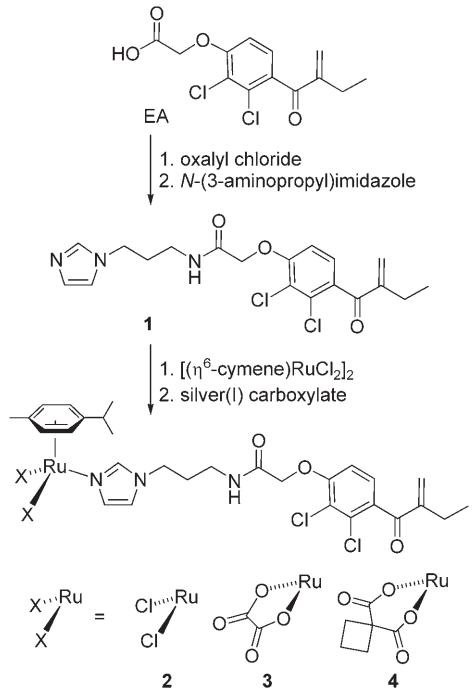

Scheme 1. Preparation of organometallic ruthenium–arene EA–imidazole complexes.

Table 1. ^{1}H and ^{13}C{^{1}H} NMR assignments [ppm] of selected resonances in complexes **2**–**4**.[a]

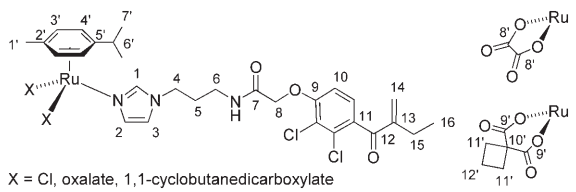

Compd	H1	H2	H3	H4	NH	H8	H1′	H6′	H7′
2	7.95	7.30	6.91	3.89	6.94	4.60	2.16	2.96	1.26
3	7.99	7.36	6.79	4.04	8.17	4.77	2.02	2.67	1.18
4	7.58	7.18	6.90	3.86	7.49	4.62	2.16	2.78	1.26

Compd	C1	C4	C8	C12	C1′	C6′	C7′	C8′	C9′
2	140.1	45.5	68.3	195.8	18.5	30.7	22.3	–	–
3	139.6	44.7	67.9	195.2	17.4	30.2	22.2	164.8	–
4	138.6	45.3	68.2	195.8	17.8	30.7	22.5	–	179.7

[a] NMR experiments were conducted in $CDCl_3$ except for those of compound **3**, which were conducted in [D_6]DMSO.

The ^{13}C{^{1}H} NMR spectra for **3** and **4** also revealed the presence of the carboxylate resonance at $\delta = 164.8$ and 179.7 ppm, respectively, which was absent for **2**. For ESIMS analyses, pseudomolecular ions corresponding to either $[M-Cl]^+$ or $[M+H]^+$ species were observed, which were analyzed using MS^2 fragmentation and isotopic modeling, confirming the molecular formula of the anticipated complexes.

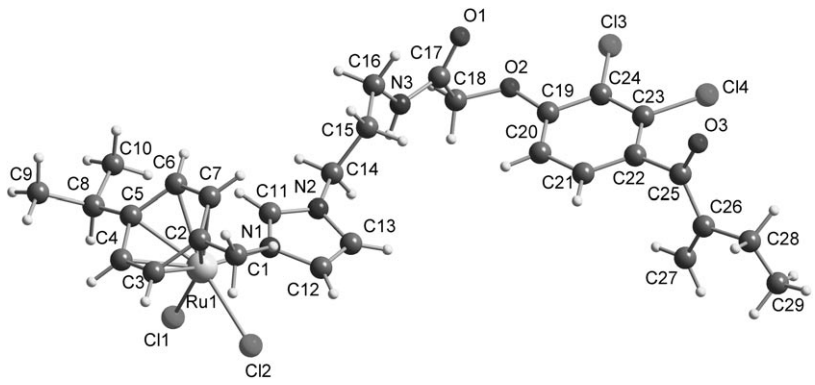

Figure 2. Ball-and-stick representation of **2**; atoms are represented by spheres of arbitrary radius. Key bond lengths [Å] and angles [°] (standard deviations given in parentheses): Ru1–C_{av} 2.192, Ru1–$cymene_{centroid}$ 1.667(4), Ru1–Cl_{av} 2.442(6); Ru1–N1, 2.133(8); N1–C11, 1.310(13); N2–C11, 1.358(12); C12–C13, 1.365(14); Cl–Ru–Cl, 88.32(10).

Single crystals of **2** suitable for X-ray crystallographic analyses were obtained by slow diffusion of Et_2O into a solution of **2** in chloroform. The structure of **2** is depicted in Figure 2, and the bond parameters are given in the caption. The key structural characteristics of the EA moiety in the EA–Im ligand are similar to those of the parent EA ligand.[14] In addition, the bond parameters around the Ru center, namely the respective Ru–$cymene_{centroid}$ and Ru–Cl distances of 1.667(4) and 2.442(6) Å are similar to other monosubstituted (η^6-cymene)ruthenium–imidazole complexes.[8,13]

GST P1-1 and the mutant forms used for the experiment were expressed in and purified from *E. coli* using a protocol reported earlier.[15] The enzymes were treated with the complexes under various incubation conditions, and the residual catalytic activity of the enzyme was determined using the CDNB–GSH assay described by Habig et al.[16] To investigate their inhibitory activity, the enzymes were treated with varying concentrations of EA and complexes **2**–**4** to determine IC_{50} values, the concentration at which 50% enzyme activity is inhibited. To determine the nature of the interaction between EA, **2**–**4**, and GST P1-1, the enzyme was treated with the compounds in the absence of GSH, and the residual activity was followed over time. In addition, samples of the treated enzyme solutions were also analyzed by ESIMS.

The ability of the ruthenium complexes to inhibit GST P1-1 activity was similar or slightly better than the parent EA (see Table 2). In contrast, both RAPTA-C and the representative (η^6-*p*-cymene)ruthenium–imidazole complex RU-A exhibited no inhibitory effect on GST P1-1, even at high concentrations. Notably, the ruthenium complex **2**, with chloride ligands, was the most efficient inhibitor of GST P1-1, more active than **3** or **4** containing chelating carboxylate ligands. In previous studies, we observed that the replacement of chloride with chelating carboxylate ligands yielded organometallic ruthenium complexes with greater aquatic stability and lower affinity towards human serum albumin and cytochrome *c*.[17] Indeed, the reported complex with the oxalate ligands was found to be less reactive than that with 1,1-cyclobutanedicarboxylate ligands, which follow a similar trend as reported herein. These new findings suggest a role of the organometallic ruthenium fragment in the inhibition of GST P1-1. Furthermore, it was observed that **2** resulted in almost complete inhibition of GST P1-1 activity (residual activity $<5\%$) at high concentrations ($>200\,\mu M$), while there was significant residual GST P1-1 activity (20%) after treatment of EA under the same concentration.

We studied the effect of treating GST P1-1 with EA and the ruthenium complexes in equimolar ratios, and monitored its activity over a period of 30 min (see Figure 3). It was observed that **2**–**4** reacted rapidly with GST P1-1, resulting in the loss of enzymatic activity. In contrast, the inactivation of GST P1-1 by EA was slower, taking 12 min for the residual activity to decrease to 50% of its original rate. In comparison, compound **2** required only 1.6 min to elicit the same effect. Moreover, GST P1-1 was inactivated more rapidly by **2** than by either of the carboxylato analogues **3** and **4**, suggesting that the ruthenium center plays a role in the inactivation of the enzyme.

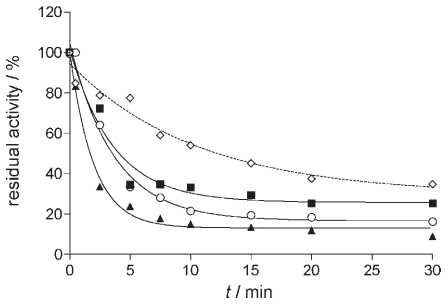

Figure 3. Inactivation of GST P1-1 activity over the course of 30 min upon treatment of EA (◇) and complexes **2** (▲), **3** (■), and **4** (○) (20 μM each).

We therefore examined the interaction of GST P1-1 with EA and **2** (see Table 2) by using GST P1-1 site-directed mutants with either Cys 101 or Cys 47 replaced by Ser residues, namely C101S and C47S. From the IC_{50} values, it is clear that both EA and **2** binding were strongly affected by the replacement of

Table 2. Inhibition of GST P1-1 and its cysteine-modified mutant forms.

Compd	Organometallic Fragment	IC_{50} [μM] wild-type	C101S	C47S
EA	–	12.0	19.4	42.9
2	[(η^6-*p*-cymene)$RuCl_2$]	8.1	22.5	36.2
3	[(η^6-*p*-cymene)Ru(C_2O_4)]	14.2	–	–
4	[(η^6-*p*-cymene)Ru($C_6H_6O_4$)]	10.6	–	–
RU-A	[(η^6-*p*-cymene)$RuCl_2$]	>200	–	–
RAPTA-C	[(η^6-*p*-cymene)$RuCl_2$]	>200	–	–

Cys47 with serine, resulting in 3.6- and 4.5-fold IC_{50} value increases, respectively. There is also some evidence that Cys101 is involved in the inhibition mechanism of **2**, with a 2.8-fold increase in IC_{50} value, whereas for EA, the increase is less marked. These data suggest that both residues are important for the inhibition of **2**, although Cys47 appears to play a more significant role. In addition, the time-course study shows that **2** is capable of inactivating the C101S mutant as efficiently as the wild-type enzyme, but not the C47S mutant (see Figure 4).

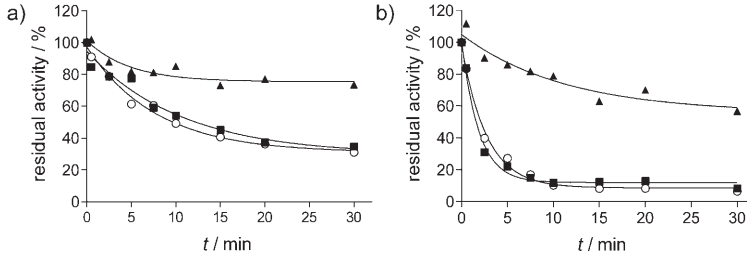

Figure 4. Inactivation of wild-type GST P1-1 and its mutant forms by a) EA and b) **2** (20 μM each) over the course of 30 min: wild-type GST P1-1 (■), GST P1-1 C101S (○), GST P1-1 C47S (▲).

Almost complete loss of activity (< 10%) in both the wild-type and C101S forms of GST P1-1 was observed after 10 min, whereas treatment with EA gave significant residual activity (> 35%) even after exposure for 30 min.

To ascertain the nature of the interaction, the enzymes were incubated with either EA or **2** and analyzed by ESIMS with a quadrupole time-of-flight (QToF) analyzer to determine the covalent adducts formed (see Figure 5). The mass peaks of 23226 Da in GST P1-1 wild-type and 23211 Da in the mutants correspond to the anticipated mass of the recombinant enzyme calculated from the cDNA sequence, whereas the respective mass peaks of 23357 and 23343 Da in wild-type and C101S mutant GST P1-1 can be attributed to the inadequate removal of the N-terminal methionine residue.[18] Upon treatment of GST P1-1 wild-type enzyme with EA, 1:1 or 1:2 covalent adducts were formed after 2 h (see Figure 5). It is known that in the absence of GSH, EA binds to GST P1-1 as a substrate in both productive and nonproductive modes, and can bind irreversibly to Cys47 via Michael addition over time. Furthermore, replacement of the cysteine residues resulted in the exclusive formation of 1:1 adducts, indicating that both Cys101 and Cys47 are involved in covalent binding. Whereas the C101S mutant reacted quantitatively with EA, substantial amounts of unreacted C47S were left after incubation with EA. This indicates that EA reacts preferentially with the Cys47 residue; this is consistent with earlier enzyme kinetics data.

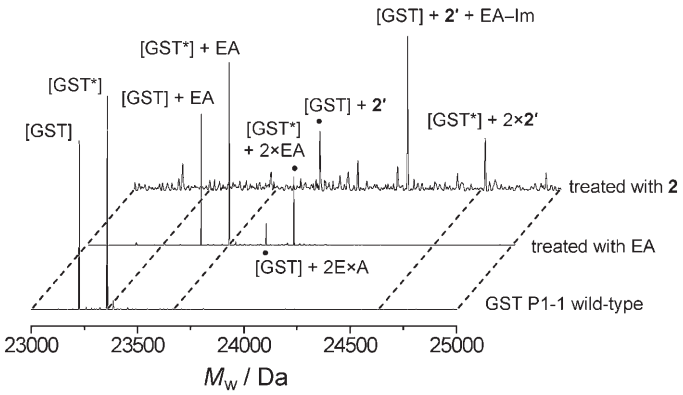

Figure 5. Deconvoluted ESIMS spectra of wild-type GST P1-1 and after treatment with EA or **2** for 2 h. [GST] corresponds to expected enzyme mass at 23226 Da, [GST*] corresponds to [GST] with uncleaved N-terminal Met residue at 23357 Da, and **2**′ is the adduct of **2** with loss of both Cl ligands; molecular mass: 644 Da.

Incubation with **2** resulted in the formation of multiple adducts containing **2** without the chloride ligands (see Table 3). The loss of the chloride ligands was anticipated because they are labile and can be substituted by other appropriate nucleophilic residues such as histidine, aspartic acid, or glutamic acid after binding to the cysteine residue. These data confirm the direct participation of the ruthenium center in binding to GST P1-1. Incubation of the C101S and C47S mutants with **2** also yielded multiple covalent adducts between the enzyme and **2** (see Figure 6). Different modes of covalent binding were observed such as the {[GST]+(η^6-*p*-cymene)Ru} adducts, which can be attributed to the replacement of the EA–Im ligand of **2** by cysteine and

Table 3. Observed mass peaks of GST P1-1 and its mutant forms incubated with EA and **2** as determined by ESI-QToF MS.

	M_w [Da]	Relative Abundance [%]	Assignment
GST P1-1 wild-type	23225	79	[GST] = [GST P1-1]
	23357	100	[GST*] = [GST P1-1]+Met
with **EA**	23530	64	[GST]+**EA**
	23661	100	[GST*]+**EA**
	23833	10	[GST]+2×**EA**
	23964	32	[GST*]+2×**EA**
with complex **2**	23226	13	[GST]
	23870	39	[GST]+2′
	24048	16	[GST]+2×**EA**−Im
	24281	100	[GST]+**2**′+**EA**−Im
	24645	29	[GST*]+2×**2**′
GST P1-1 C47S	23210	100	[C47S]
with **EA**	23211	51	[C47S]
	23514	100	[C47S]+**EA**
with complex **2**	23210	76	[C47S]
	23444	34	[C47S]+(η^6-*p*-cymene)Ru
	23621	45	[C47S]+**EA**−Im
	23854	100	[C47S]+**2**′
GST P1-1 C101S	23212	100	[C101S]
	23343	41	[C101S*] = [C101S]+Met
with **EA**	23514	100	[C101S]+**EA**
	23645	48	[C101S*]+**EA**
with complex **2**	23210	18	[C101S]
	23444	10	[C101S]+(η^6-*p*-cymene)Ru
	23621	27	[C101S]+**EA**−Im
	23854	64	[C101S]+**2**′
	24265	100	[C101S*]+**2**′+**EA**−Im

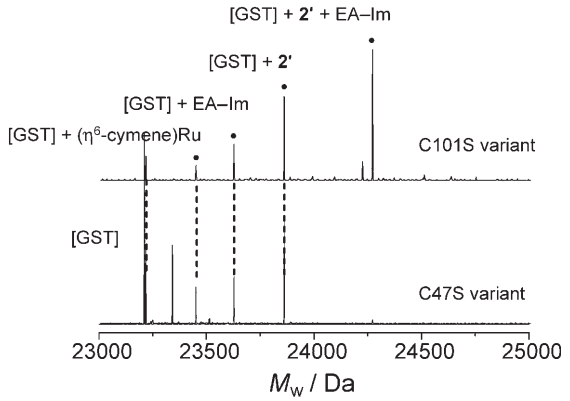

Figure 6. Deconvoluted ESIMS spectra of GST P1-1 C101S (top) and GST P1-1 C47S (bottom) after treatment with **2** for 2 h. [GST] corresponds to parent enzyme mutant at mass 23 211 Da, [GST*] corresponds to the enzyme with uncleaved *N*-terminal Met residue at 23 343 Da, and **2**′ is the adduct of **2** with loss of both Cl ligands, namely [(η^6-*p*-cymene)Ru(EA–Im)], with a molecular mass of 644 Da.

other nucleophilic residues. As with EA, C47S was less reactive towards **2** than C101S, with significant amounts of unreacted C47S enzyme left after incubation. In addition, the {[GST]+**2**′+EA–Im} adduct was observed with C101S and not with C47S (see Table 3), indicating that the integrity of the catalytic site is important for the binding of **2** to GST P1-1.

It is evident that while both Cys 47 and Cys 101 residues are involved in the covalent binding of **2** to GST P1-1, kinetic studies and ESIMS data show that the binding to Cys 47 has a stronger inactivation effect. A possible explanation is that the main mode of inhibition of **2** is similar to that of EA, through competitive binding to the H site against electrophilic substrates, as indicated by the similar IC_{50} values determined for wild-type GST P1-1. However, the organometallic Ru fragment in **2** is also capable of reacting at the Cys 47 residue and, to a lesser extent, Cys 101, resulting in rapid inactivation of the enzyme. Lower rates of inactivation of the wild-type enzyme are also observed with the less reactive carboxylato complexes **3** and **4**.

The efficacy at which the complexes inhibit cancer cell growth was evaluated against the cisplatin-sensitive A2780 and the cisplatin-resistant A2780cisR human ovarian carcinoma cell lines (see Table 4). Both cell lines were shown to express similar amounts of GST Pi by Western blot experiments (see Figure 7). The ruthenium complexes were highly active in inhibiting the growth of both ovarian carcinoma cell lines; they were 10-fold more efficient than the well-established RAPTA-C and the representative (η^6-*p*-cymene)ruthenium–imidazole complex RU-A, and 3–5-fold more efficient than EA on a molar basis. The good correlation between their ability to inhibit cancer cell growth and their ability to inhibit GST activity amongst EA and the ruthenium complexes indicates that GST Pi may be an important intracellular target of these complexes.

Table 4. Inhibition of viability of A2780 and A2780cisR ovarian carcinoma cell lines upon treatment with the test complexes.

Compd	IC_{50} [μM][a]	
	A2780 [μM]	A2780cisR [μM]
EA	57.9 ± 1.1	54.5 ± 1.4
2	10.3 ± 2.1	12.9 ± 1.1
3	16.6 ± 1.4	9.4 ± 0.4
4	15.6 ± 0.9	9.8 ± 0.6
RU-A	> 100	> 100
RAPTA-C	> 200	> 200

[a] Period of drug exposure: 72 h; cell viability determined using the MTT assay.

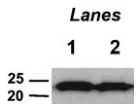

Figure 7. Western blot evaluation of the expression of Pi by A2780cisR (lane 1) and A2780 (lane 2). Similar protein loading of both cell extracts was ascertained by tubulin immunodetection (results not shown).

Conclusions

A series of organometallic (η^6-*p*-cymene)ruthenium-based GST inhibitors containing the ethacrynic acid functionality were developed. As with EA, they are effective inhibitors of GST P1-1, but they interact with GST P1-1 differently. The ruthenium complexes rapidly inactivate the enzyme, and an investigation using the cysteine-modified mutants revealed that covalent binding occurs at Cys 47 and, to a lesser extent, at the Cys 101 residue. They are also effective inhibitors of the growth of human ovarian cancer cell lines, irrespective of cisplatin resistance, and the data suggest that GST P1-1 is the possible target of these complexes in vitro.

Experimental Section

All reagents were purchased from Acros unless otherwise indicated. EA and GSH were purchased from Sigma, hydrated $RuCl_3$ from Precious Metals Online, *n*-butylimidazole from Lancaster, and cell culture reagents were obtained from Gibco–BRL, Basel, Switzerland. The reactions were performed with solvents dried using appropriate reagents and distilled prior to use. [(η^6-*p*-cymene)RuCl(μ-Cl)]$_2$ was prepared and purified according to literature procedures.[19] NMR spectra were measured on a Bruker DMX 400 instrument at 20 °C using the residual solvent resonance as internal standard. ESIMS data for synthesized compounds were recorded on a Thermo Finnigan LCQ Deca XP Plus quadrupole ion trap instrument in positive mode with ionization energy set at 5.0 V and capillary temperature at 150 °C, using CH_3CN as the solvent.[20] UV/Vis measurements were conducted on a Varian Cary 4000 UV/Vis spectrophotometer equipped with a thermostatic cuvette compartment. Elemental analyses were carried out at the Institute of Chemical Sciences and Engineering, EPFL.

Synthesis of EA–imidazole 1: EA (349 mg, 1.16 mmol) was held at reflux in CH_2Cl_2 (20 mL) with an excess of oxalyl chloride (2 mL) for 1 h. Unreacted oxalyl chloride was removed under vacuum, and the reaction mixture was concentrated to yield ethacrynic acid chloride as a colorless oil. The acid chloride was dissolved in CH_2Cl_2 (20 mL) and *N*-(aminopropyl)imidazole (500 mg, 4.00 mmol) was added. The reaction mixture was then held at reflux for 2 h. A solution of $NaHCO_3$ (5%, 25 mL) was added to quench the reaction, and the aqueous phase was extracted with CH_2Cl_2 (3 × 25 mL). The

organic phases were combined and washed with brine (2×25 mL) and dried over Na_2SO_4. The solvent was removed, and the product was separated on silica using EtOH/$CHCl_3$ 2:8 as eluent. The solvent was removed to yield a colorless oil (yield: 378 mg, 80%). ^{1}H NMR (400 MHz, $CDCl_3$): δ = 7.52 (s, 3H, H1), 7.07 (s, 3H, H2), 6.96 (s, 3H, H3), 7.20 (d, $^3J_{(H,H)}$ = 8.4 Hz, 1H, H9), 6.86 (d, $^3J_{(H,H)}$ = 8.4 Hz, 1H, H9), 6.82 (m, 1H, NH), 5.96 (s, 1H, H14), 5.59 (s, 1H, H14), 4.57 (s, 2H, H7), 4.04 (t, $^3J_{(H,H)}$ = 7.2 Hz, 2H, H4), 3.42 (q, $^3J_{(H,H)}$ = 7.2 Hz, 2H, H6), 2.47 (q, $^3J_{(H,H)}$ = 7.6 Hz, 2H, H15), 2.10 (m, 2H, H5), 1.16 ppm (t, $^3J_{(H,H)}$ = 7.6 Hz, 3H, H16).

Synthesis of (η^6-*p*-cymene)$RuCl_2$(EA–imidazole) 2: [(η^6-*p*-cymene)RuCl(μ-Cl)]$_2$ (68 mg, 0.11 mmol) and freshly prepared EA–imidazole (94 mg, 0.23 mmol) were dissolved in CH_2Cl_2 (10 mL) and stirred for 12 h. The reaction mixture was concentrated to ~5 mL, and pentane (20 mL) was added to precipitate the product. The product was recrystallized from CH_2Cl_2/pentane to yield an orange solid (yield: 144 mg, 90%). Vapor diffusion of Et_2O into a $CHCl_3$ solution of **2** yielded crystals suitable for X-ray crystallographic analyses. ^{1}H NMR (400 MHz, $CDCl_3$): δ = 7.95 (s, 1H, H1), 7.30 (s, 1H, H2), 6.91 (s, 1H, H3), 7.19 (d, $^3J_{(H,H)}$ = 8.4 Hz, 1H, H9), 6.90 (d, $^3J_{(H,H)}$ = 8.4 Hz, 1H, H9), 6.94 (m, 1H, NH), 5.96 (s, 1H, H14), 5.61 (s, 1H, H14), 5.45 (d, $^3J_{(H,H)}$ = 6.0 Hz, 2H, H3′), 5.26 (d, $^3J_{(H,H)}$ = 6.0 Hz, 2H, H4′), 4.60 (s, 2H, H8), 3.89 (t, $^3J_{(H,H)}$ = 7.2 Hz, 2H, H4), 3.36 (q, $^3J_{(H,H)}$ = 7.2 Hz, 2H, H6), 2.96 (septet, $^3J_{(H,H)}$ = 8.0 Hz, 1H, H6′), 2.47 (q, $^3J_{(H,H)}$ = 7.6 Hz, 2H, H15), 2.16 (s, 3H, H1′), 1.93 (m, 2H, H5), 1.26 (d, $^3J_{(H,H)}$ = 8.0 Hz, 6H, H7′), 1.15 ppm (t, $^3J_{(H,H)}$ = 7.6 Hz, 3H, H16); ^{13}C{^{1}H} NMR (100 MHz, $CDCl_3$): δ = 195.8 (C12), 167.4 (C7), 155.1 (C9), 150.2 (C13), 140.1 (C1), 133.9 (C11), 131.9 (C2), 119.5 (C3), 128.8 (C14), 127.2 111.2 (2×C10), 102.7 (C5′), 97.3 (C2′), 82.6 (C4′), 81.4 (C3′), 68.3 (C8), 45.5 (C4), 35.9 (C6), 30.7 (C6′), 30.7 (C5), 23.4 (C15), 22.3 (C7′), 18.5 (C1′), 12.4 ppm (C16); ESIMS: *m/z*: 682 [M^+−Cl]; anal. ($C_{29}H_{35}Cl_4N_3O_3Ru$): C 48.67, H 4.93, N 5.88, found: C 48.75, H 4.95, N 5.79.

Synthesis of (η^6-*p*-cymene)Ru(C_2O_4)(EA–imidazole) 3: [(η^6-*p*-cymene)RuCl(μ-Cl)]$_2$ (197 mg, 0.322 mmol) and silver oxalate (240 mg, 0.797 mmol) were stirred in H_2O for 2 h. The mixture was filtered through celite to remove the AgCl precipitate. The solvent was removed under vacuum, and the residue was redissolved in methanol (25 mL). Freshly prepared EA–imidazole (94 mg, 0.23 mmol) was added, and the reaction was stirred for 12 h. The reaction mixture was concentrated to 5 mL, and pentane (20 mL) was added to precipitate the product. The product was recrystallized from CH_2Cl_2/pentane to yield a pale-yellow solid (yield: 401 mg, 85%). ^{1}H NMR (400 MHz, [D$_6$]DMSO): δ = 8.17 (m, 1H, NH), 7.99 (s, 1H, H1), 7.36 (s, 1H, H2), 6.79 (s, 1H, H3), 7.35 (d, $^3J_{(H,H)}$ = 8.8 Hz, 1H, H10), 7.11 (d, $^3J_{(H,H)}$ = 8.8 Hz, 1H, H10), 5.96 (s, 1H, H14), 5.55 (s, 1H, H14), 5.71 (d, $^3J_{(H,H)}$ = 5.6 Hz, 2H, H3′), 5.48 (d, $^3J_{(H,H)}$ = 5.6 Hz, 2H, H4′), 4.77 (s, 2H, H8), 4.04 (t, $^3J_{(H,H)}$ = 7.2 Hz, 2H, H4), 3.08 (q, $^3J_{(H,H)}$ = 7.2 Hz, 2H, H6), 2.67 (septet, $^3J_{(H,H)}$ = 8.0 Hz, 1H, H6′), 2.37 (q, $^3J_{(H,H)}$ = 7.2 Hz, 2H, H15), 2.02 (s, 3H, H1′), 1.88 (m, 2H, H5), 1.18 (d, $^3J_{(H,H)}$ = 6.8 Hz, 6H, H7′), 1.07 ppm (t, $^3J_{(H,H)}$ = 7.2 Hz, 3H, H16); ^{13}C{^{1}H} NMR (100 MHz, [D$_6$]DMSO): δ = 195.2 (C12), 166.9 (C7), 164.8 (C8′), 155.6 (C9), 149.4 (C13), 139.6 (C1), 132.5 (C11), 129.5 (C14), 128.7 (C2), 120.6 (C3), 127.7 112.0 (2×C10), 99.4 (C5′), 96.7 (C2′), 82.6 (C4′), 79.0 (C3′), 67.9 (C8), 44.7 (C4), 35.2 (C6), 30.5 (C5), 30.2 (C6′), 22.9 (C15), 22.2 (C7′), 17.4 (C1′), 12.4 (C16); ESIMS: *m/z*: 734 [M^++H], 756 [M^++Na], 1490 [M_2^++Na]; anal. ($C_{31}H_{35}Cl_2N_3O_7Ru$): C 50.75, H 4.81, N 5.73, found: C 50.39, H 4.83, N 5.48.

Synthesis of (η^6-*p*-cymene)Ru($C_6H_6O_4$)(EA–imidazole) 4: [(η^6-*p*-cymene)RuCl(μ-Cl)]$_2$ (228 mg, 0.373 mmol) and silver 1,1-cyclobutanedicarboxylate (300 mg, 0.838 mmol) were stirred in CH_3CN (50 mL) for 12 h, during which a yellow precipitate was formed. The solvent was removed, and the residue was redissolved in methanol (25 mL). The mixture was filtered through celite to remove the AgCl precipitate. Freshly prepared EA–imidazole (94 mg, 0.23 mmol) was added to the filtrate, and the reaction was stirred for 12 h. The reaction mixture was concentrated to 5 mL, and pentane (20 mL) was added to precipitate the product. The product was recrystallized from CH_2Cl_2/pentane to yield a bright-yellow solid (yield: 440 mg, 75%). ^{1}H NMR (400 MHz, $CDCl_3$): δ = 7.58 (s, 1H, H1), 7.18 (s, 1H, H2), 6.90 (s, 1H, H3), 7.17 (d, $^3J_{(H,H)}$ = 7.2 Hz, 1H, H10), 6.90 (d, $^3J_{(H,H)}$ = 7.2 Hz, 1H, H10), 7.49 (m, 1H, NH), 5.95 (s, 1H, H14), 5.60 (s, 1H, H14), 5.46 (d, $^3J_{(H,H)}$ = 6.0 Hz, 2H, H3′), 5.26 (d, $^3J_{(H,H)}$ = 6.0 Hz, 2H, H4′), 4.62 (s, 2H, H8), 3.86 (t, $^3J_{(H,H)}$ = 6.4 Hz, 2H, H4), 3.14 (q, $^3J_{(H,H)}$ = 6.4 Hz, 2H, H6), 2.78 (septet, $^3J_{(H,H)}$ = 6.8 Hz, 1H, H6′), 2.59 (t, $^3J_{(H,H)}$ = 7.6 Hz, 2H, H11′), 2.50 (t, $^3J_{(H,H)}$ = 7.6 Hz, 2H, H11′), 2.45 (q, $^3J_{(H,H)}$ = 6.4 Hz, 2H, H15), 2.16 (s, 3H, H1′), 1.95 (m, 2H, H5), 1.82 (t, $^3J_{(H,H)}$ = 7.6 Hz, 2H, H12′), 1.26 (d, $^3J_{(H,H)}$ = 6.8 Hz, 6H, H7′), 1.20 (t, $^3J_{(H,H)}$ = 7.6 Hz, 3H, H16); ^{13}C{^{1}H} NMR (100 MHz, $CDCl_3$): δ = 195.8 (C12), 179.7 (C9′), 167.7 (C7), 155.1 (C9), 150.2 (C13), 138.6 (C1), 133.8 (C11), 130.4 (C2), 119.9 (C3), 128.9 (C14), 127.2 111.1 (2×C10), 100.0 (C5′), 97.4 (C2′), 82.1 (C4′), 80.1 (C3′), 68.2 (C8), 55.7 (C10′), 45.3 (C4), 35.7 (C6), 35.0 26.7 (2×C11′), 30.7 (C6′), 29.9 (C5), 23.3 (C15), 22.5 (C7′), 17.8 (C1′), 15.5 (C12′), 12.4 (C16); ESIMS: *m/z*: 788 [M^++H], 1198 [M^++EA−imidazole+H], 410 [EA$^+$−imidazole+H]; anal. ($C_{35}H_{41}Cl_2N_3O_7Ru$): C 53.37, H 5.25, N 5.34, found: C 53.17, H 5.37, N 5.25.

Synthesis of (η^6-*p*-cymene)$RuCl_2$(*n*-butylimidazole) RU-A: The synthesis was adapted from a published method.[8] [(η^6-*p*-cymene)RuCl(μ-Cl)]$_2$ (247 mg, 0.40 mmol) was added to *n*-butylimidazole (100 μL, 95 mg, 0.76 mmol) in toluene (20 mL). The reaction was sonicated in an ultrasound bath for 2 h, during which an orange precipitate was formed. The precipitate was filtered, washed with cold toluene (20 mL) and Et_2O (20 mL), and dried in vacuo to yield an orange solid (yield: 173 mg, 50%). ^{1}H NMR (400 MHz, $CDCl_3$): δ = 7.98 (s, 1H, H1), 7.30 (s, 1H, H2), 6.87 (s, 1H, H3), 5.43 (d, $^3J_{(H,H)}$ = 6.0 Hz, 2H, H3′), 5.24 (d, $^3J_{(H,H)}$ = 6.0 Hz, 2H, H4′), 3.87 (t, $^3J_{(H,H)}$ = 7.2 Hz, 2H, *n*-butyl-H4), 2.96 (septet, $^3J_{(H,H)}$ = 6.8 Hz, 1H, H6′), 2.18 (s, 3H, H1′), 1.73 (m, 2H, *n*-butyl-H5), 1.32 (m, 2H, *n*-butyl-H6), 1.27 (d, $^3J_{(H,H)}$ = 6.8 Hz, 6H, H7′), 0.93 (t, $^3J_{(H,H)}$ = 7.2 Hz, 3H, *n*-butyl-CH_3); ESIMS: *m/z*: 395 [M^+−Cl], 437 [M^+−Cl+CH_3CN], 520 [M^+−Cl+butyl−imidazole].

Structural characterization of 2 in the solid state: Graphic representation is given in Figure 1, and selected bond distances and angles are given in the caption. Data collection was performed on a Bruker–Nonius KappaCDD diffractometer. The unit cell and orientation matrix were determined by indexing reflections measured from a sampling of scan and analyzed with DirAX.[21] Data collection were performed by scanning reflections from the entire Ewald sphere using the program CollectCCD,[22] and data reduction was carried out with EvalCCD.[23] Structure solution was performed using SiR92,[24] and the structure was refined by full-matrix least-squares refinement (against F^2) using SHELXTL software.[25] All non-hydrogen atoms were refined anisotropically while hydrogen atoms were placed in their geometrically generated positions and refined using the riding model. A multi-scan absorption correction based on a semiempirical method was applied using SADABS.[26] Graphical representations of the structure were made with Diamond.[27] CCDC 646167 contains the supplementary crystallographic data for this paper. These data can be obtained free of charge from The Cambridge Crystallographic Data Centre via www.ccdc.cam.ac.uk/data request/cif.

Crystal data for 2: $C_{29}H_{35}Cl_4N_3O_3Ru$, $M_w = 716.47$, crystal system = monoclinic, $a = 21.250(18)$ Å, $b = 8.692(4)$ Å, $c = 17.017(7)$ Å, $\alpha = \gamma = 90°$, $\beta = 105.75(4)°$, $V = 3025(3)$ Å^3, $T = 100(2)$ K, space group = $P2_1/c$, $Z = 4$, ($Mo_{K\alpha}$) = 0.71073 Å, 27455 reflections collected, 4880 independent reflections, $R_{int} = 0.1128$, $R1$ $[I > 2(I)] = 0.0938$, $wR2$ (all data) = 0.2067.

Protein expression and purification: Human GST P1-1 wild-type and the C47S and C101S mutants were expressed in *E. coli* and purified as previously described.[15] Briefly, TOP10 *E. coli* cells, harboring plasmid pGST-1, were grown in LB medium containing 100 μg mL^{-1} ampicillin and 50 μg mL^{-1} streptomycin. The expression of GST was induced by the addition of 0.2 mM isopropyl-1-thio-β-galactopyranoside when the absorbance value at 600 nm reached 0.5. The cells were harvested and lysed 18 h after induction. GST P1-1 and the cysteine-modified mutants were purified by affinity chromatography on immobilized glutathione. Enzymatic activity was determined by measuring the rate of the conjugation reaction between 1 mM CDNB and 1 mM GSH in 1 mL of 100 mM phosphate buffer pH 6.5 at 25 °C. The reaction was monitored spectrophotometrically at 340 nm corresponding to the absorbance maxima of glutathione-2,4-dinitrobenzene conjugate ($\varepsilon_{340} = 9.6\ M^{-1}cm^{-1}$).

Inhibition of GST P1-1 activity by EA and complexes 2–4: Varying concentrations of EA and complexes **2–4** (0.1–200 μM), pre-dissolved in DMSO (10 mM) were added to reaction mixtures containing 1 mM GSH in 100 mM phosphate buffer pH 6.5 and 44 nM GST P1-1 enzyme. The residual activity of wild-type GST P1-1 and its mutant forms was assayed spectrophotometrically upon addition of the CDNB substrate (final concentration 1 mM). The IC_{50} values for the inhibition of GST activity were determined by fitting the plot of residual GST activity against the inhibitor concentrations with a sigmoidal dose–response function using Prism (GraphPad).

Time-course inactivation by EA and complexes 2–4: GST P1-1 and its mutant forms (20 μM) were incubated with EA and **2–4** (20 μM), pre-dissolved in DMSO, in 10 mM phosphate buffer pH 7.0 at 37 °C. At fixed time intervals, over a period of 30 min, aliquots of the sample mixture were assayed for residual GST activity in 100 mM phosphate buffer pH 6.5 containing 1 mM GSH and 1 mM CDNB.

Analyses of binding of EA and 2 to GST P1-1 enzymes by ESI-QToF MS: GST P1-1 and its mutant forms (5 μM) were incubated with either EA or **2** (10 μM) in phosphate buffer pH 7.0 at 37 °C for 2 h. The samples were purified using the stream-select module (CapLC, Waters) before ESIMS analyses. Briefly, samples (1.4 μL) were loaded onto a C_{18} pre-column (Symmetry, Waters), washed with a solution of 2% CH_3CN and 0.1% formic acid for 3 min, eluted with a solution of 98% CH_3CN and 0.1% formic acid for 7 min in reverse flow, and analyzed by ESI-QToF MS (Micromass) at *m/z* 500–4000. Spectral data were processed and deconvoluted with the MassLynx/MaxENT1 software package.

Cell culture and inhibition of cell growth: Human A2780 and A2780cisR ovarian carcinoma cell lines were obtained from the European Centre of Cell Cultures (ECACC, Salisbury, UK) and maintained in culture as described by the provider. The cells were routinely grown in RPMI 1640 medium containing 10% fetal calf serum (FCS) and antibiotics at 37 °C and 6% CO_2. For the evaluation of growth inhibition tests, the cells were seeded in 96-well plates (Costar, Integra Biosciences, Cambridge, USA) and grown for 24 h in complete medium. EA and complexes **2–4** were pre-dissolved in DMSO at 100 mM, diluted in culture medium to the required concentration, and added to the cell culture for further 72 h incubation. The MTT test was performed for the last 2 h without changing the culture medium.[28] Briefly, following drug exposure, MTT (3-[4,5-dimethylthiazol-2-yl]-2,5-diphenyltetrazolium bromide, Sigma) was added to the cells at a final concentration of 0.2 mg mL^{-1} and incubated for 2 h. The culture medium was then aspirated, and the violet formazan precipitate was dissolved in 0.1 N HCl in 2-propanol. The optical density was quantified at 540 nm using a multi-well plate reader (iEMS Reader MF, Labsystems, USA), and the percentage of surviving cells was calculated from the ratio of absorbance of treated to untreated cells. The IC_{50} values for the inhibition of cell growth were determined by fitting the plot of the percentage of surviving cells against the drug concentration using a sigmoidal function (Origin v 7.5).

Western blot analysis: Human A2780 and A2780cisR ovarian carcinoma cells were grown in Petri dishes (∅ = 6 cm, BD Falcon) until they reached 80–100% confluence. They were then washed with sterile phosphate-buffered saline (PBS) and extracted in lysis buffer (50 mM Tris·HCl, 150 mM NaCl, 2 mM EDTA, 0.5% Triton-X100 *v/v*) containing protease cocktail inhibitors (Roche) by 5 cycles of freezing and thawing, and then centrifuged at 16000 *g* at 4 °C. Protein concentration of the cytosol extract was determined using the BCA assay (Pierce) using bovine serum albumin (BSA) as reference. The cytosolic proteins were resolved on 15% polyacrylamide gels and transferred onto a nitrocellulose membrane (Schleicher & Schuell). GST Pi was determined using a polyclonal rabbit anti-GST Pi antibody (Stressgen, diluted 1:1000) and anti-rabbit antibody conjugated to horseradish peroxidase (Promega, diluted 1:5000) with enhanced chemiluminescence detection (ECL plus, Amersham). For protein loading control (results not shown), the membrane was re-hybridized with monoclonal mouse anti-tubulin antibody (Abcam, diluted 1:5000) and anti-mouse antibody conjugated to horseradish peroxidase (Sigma, diluted 1:5000) with enhanced chemiluminescence detection (ECL plus, Amersham).

Acknowledgements

The authors thank Dr. Rosario Scopelliti (EPFL) and Dr. Euro Scolari (EPFL) for carrying out data collection for the X-ray diffraction analysis, and Dr. Alain Razaname (EPFL) for assistance in the recording of mass spectra.

Keywords: anticancer drugs · bioorganometallic chemistry · ethacrynic acid · mass spectrometry · ruthenium

[1] W. H. Habig, W. B. Jakoby, *Methods Enzymol.* **1981**, *77*, 218–231.
[2] D. M. Townsend, V. L. Findlay, K. D. Tew, *Methods Enzymol.* **2005**, *401*, 287–307.
[3] K. D. Tew, Z. Ronai, *Drug Resist. Updates* **1999**, *2*, 143–147.
[4] J. D. Hayes, J. U. Flanagan, I. R. Jowsey, *Ann. Rev. Pharmacol. Toxicol.* **2005**, *45*, 51–88.
[5] M. C. J. Wilce, M. W. Parker, *Biochim. Biophys. Acta* **1994**, *1205*, 1–18.
[6] M. Lo Bello, A. Pastore, R. Petruzzelli, M. W. Parker, M. C. J. Wilce, G. Federici, G. Ricci, *Biochem. Biophys. Res. Commun.* **1993**, *194*, 804–810.
[7] G. Ricci, G. Del Boccio, A. Pennelli, M. Lo Bello, R. Petruzzelli, A. M. Caccuri, D. Barra, G. Federici, *J. Biol. Chem.* **1991**, *266*, 21409–21415.
[8] C. A. Vock, C. Scolaro, A. D. Phillips, R. Scopelliti, G. Sava, P. J. Dyson, *J. Med. Chem.* **2006**, *49*, 5552–5561.
[9] a) C. Scolaro, T. J. Geldbach, S. Rochat, A. Dorcier, C. Gossens, A. Bergamo, M. Cocchietto, I. Tavernelli, G. Sava, U. Rothlisberger, P. J. Dyson, *Organometallics* **2006**, *25*, 756–765; b) C. Scolaro, A. Bergamo, L. Brescacin, R. Delfino, M. Cocchietto, G. Laurenczy, T. J. Geldbach, G. Sava, P. J. Dyson, *J. Med. Chem.* **2005**, *48*, 4161–4171; c) C. S. Allardyce, P. J. Dyson, D. J. Ellis, S. L. Heath, *Chem. Commun.* **2001**, 1396–1397.

[10] W. H. Ang, P. J. Dyson, *Eur. J. Inorg. Chem.* **2006**, 4003 – 4018.
[11] W. H. Ang, I. Khalaila, C. S. Allardyce, L. Juillerat-Jeanneret, P. J. Dyson, *J. Am. Chem. Soc.* **2005**, *127*, 1382 – 1383.
[12] a) D. A. Koechel, E. J. Cafruny, *J. Med. Chem.* **1973**, *16*, 1147 – 1152; b) G. S. Zhao, T. Yu, R. Wang, X. B. Wang, Y. K. Jing, *Bioorg. Med. Chem.* **2005**, *13*, 4056 – 4062.
[13] C. A. Vock, W. H. Ang, C. Scolaro, A. D. Phillips, L. Lagopoulos, L. Juillerat-Jeanneret, G. Sava, R. Scopelliti, P. J. Dyson, *J. Med. Chem.* **2007**, *50*, 2166 – 2175.
[14] J. Lamotte, H. Campsteyn, L. Dupont, M. Vermeire, *Acta Crystallogr. Sect. B* **1978**, *34*, 2636 – 2638.
[15] a) A. Battistoni, A. P. Mazzetti, R. Petruzzelli, M. Muramatsu, G. Federici, G. Ricci, M. Lo Bello, *Protein Expression Purif.* **1995**, *6*, 579 – 587; b) M. Lo Bello, A. Battistoni, A. P. Mazzetti, P. G. Board, M. Muramatsu, G. Federici, G. Ricci, *J. Biol. Chem.* **1995**, *270*, 1243 – 1253.
[16] W. H. Habig, M. J. Pabst, W. B. Jakoby, *J. Biol. Chem.* **1974**, *249*, 7130 – 7139.
[17] a) W. H. Ang, E. Daldini, C. Scolaro, R. Scopelliti, L. Juillerat-Jeannerat, P. J. Dyson, *Inorg. Chem.* **2006**, *45*, 9006 – 9013; b) A. Casini, G. Mastrobuoni, W. H. Ang, C. Gabbiani, G. Pieraccini, G. Moneti, P. J. Dyson, L. Messori, *ChemMedChem* **2007**, *2*, 631 – 635.
[18] M. Lo Bello, M. Nuccetelli, A. M. Caccuri, L. Stella, M. W. Parker, J. Rossjohn, W. J. McKinstry, A. F. Mozzi, G. Federici, F. Polizio, J. Z. Pedersen, G. Ricci, *J. Biol. Chem.* **2001**, *276*, 42138 – 42145.
[19] M. A. Bennett, A. K. Smith, *J. Chem. Soc. Dalton Trans.* **1974**, 233 – 241.
[20] P. J. Dyson, J. S. McIndoe, *Inorg. Chim. Acta* **2003**, *354*, 68 – 74.
[21] A. J. M. Duisenberg, *J. Appl. Crystallogr.* **1992**, *25*, 92 – 96.
[22] R. W. W. Hooft, *CollectCCD*, Nonius BV, Delft (Netherlands).
[23] A. J. M. Duisenberg, L. M. J. Kroon-Batenburg, A. M. M. Schreurs, *J. Appl. Crystallogr.* **2003**, *36*, 220 – 229.
[24] A. Altomare, G. Cascarano, C. Giacovazzo, A. Guagliardi, *J. Appl. Crystallogr.* **1993**, *26*, 343 – 350.
[25] CrysAlis CCD and CrysAlis RED, Versions 1.170, 2003, Oxford Diffraction Ltd., Abingdon, OX144 RX (UK).
[26] G. M. Sheldrick, SADABS, Program for Empirical Absorption Correction of Area Detector Data, 1996, Universität Göttingen, Göttingen (Germany).
[27] Diamond 3.0a, Crystal Impact GbR, 2004, Bonn, (Germany).
[28] a) T. Mosmann, *J. Immunol. Methods* **1983**, *65*, 55 – 63; b) W. H. Ang, S. Pilet, R. Scopelliti, F. Bussy, L. Juillerat-Jeanneret, P. J. Dyson, *J. Med. Chem.* **2005**, *48*, 8060 – 8069.

Received: May 28, 2007
Revised: August 22, 2007
Published online on October 8, 2007

